Geomorphometry of Cerro Sillajhuay (Andes, Chile/Bolivia): Comparison of Digital Elevation Models (DEMs) from ASTER Remote Sensing Data and Contour Maps

Ulrich Kamp
Department of Geography and Environmental Science Program, DePaul University
990 W Fullerton Ave, Chicago, IL 60614-2458, U.S.A.
E-mail: ukamp@depaul.edu

Tobias Bolch
Department of Geography, Humboldt University Berlin
Rudower Chausse 16, Unter den Linden 6, 10099 Berlin, Germany
E-mail: tobias.bolch@email.de

Jeffrey Olsenholler
Department of Geography and Geology, University of Nebraska - Omaha
6001 Dodge Street, Omaha, NE 68182-0199, U.S.A.
jolsenho@cosmos.unomaha.edu

Abstract

Digital elevation models (DEMs) are increasingly used for visual and mathematical analysis of topography, landscapes and landforms, as well as modeling of surface processes. To accomplish this, the DEM must represent the terrain as accurately as possible, since the accuracy of the DEM determines the reliability of the geomorphometric analysis. For Cerro Sillajhuay in the Andes of Chile/Bolivia two DEMs are compared: one derived from contour maps, the other from a satellite stereo-pair from the Advanced Spaceborne Thermal Emission and Reflection Radiometer (ASTER). As both DEM procedures produce estimates of elevation, quantative analysis of each DEM was limited. The original ASTER DEM has a horizontal resolution of 30 m and was generated using tie points (TPs) and ground control points (GCPs). It was then resampled to 15 m resolution, the resolution of the VNIR bands. Five parameters were calculated for geomorphometric interpretation: elevation, slope angle, slope aspect, vertical curvature, and tangential curvature. Other calculations include flow lines and solar radiation. Although elevations are too low above 5000 m asl., the ASTER DEM offers reliable results when analyzing the macro- and mesorelief, and for mapping at medium scales (1:100,000 to 1:50,000).

Introduction

Digital elevation models (DEMs) are increasingly used for visual and mathematical analysis of topography, landscapes and landforms, as well as modeling of surface processes (Bishop and Shroder, 2000; Dikau *et al.*, 1995; Giles, 1998; Millaresis and Argialas, 2000; Tucker *et al.*, 2001). DEMs play also an important tool for the analysis of glaciers and glaciated terrains (Baral and Gupta, 1997; Duncan *et al.*, 1998; Etzelmüller and Sollid, 1997; Lodwick and Paine, 1985; Sidjak and Wheate, 1999; Theakstone and Jacobsen, 1997). Bishop *et al.* (2002) used a DEM of Nanga Parbat to map glaciers in the rough mountain terrain of the western Himalayas. Gratton *et al.* (1993) calculated the net radiation field of mountain glacier outlets in the Rocky Mountains from a DEM.

A DEM offers the most common method for extracting vital topographic information and even enables the modeling of flow across topography, a controlling factor in distributed models of landform processes (Dietrich *et al.*, 1993; Desmet and Govers, 1995; Kirkby, 1990). To accomplish this, the DEM must represent the terrain as accurately as possible, since the accuracy of the DEM determines the reliability of the geomorphometric analysis. Currently, the automatic generation of a DEM from remotely sensed data with sub-pixel accuracy is possible (Krzystek, 1995). A number of researchers have studied the effects of DEM resolution on the estimation of topography (Band *et al.*, 1995; Chang and Tsai, 1991; Gao, 1997; Hodgson, 1995; Schoorl *et al.*, 2000; Stefanovic and Wiersema, 1985).

DEMs can be generated from electro-optic scanners such as ASTER (Advanced Spaceborne Thermal Emission and

Reflection Radiometer). ASTER offers simultaneous along-track stereo-pairs, which eliminate variations caused by multi-date stereo data acquisition. Only some results have been published in peer-reviewed literature about using ASTER data yet, mostly on simulated ASTER data (Abrams and Hook, 1995; Shi, 2001, Welch *et al.*, 1998), or on the potential of using ASTER data in the future (Raup *et al.*, 2000). Kääb (2002) and Kääb *et al.* (2002) used ASTER images for a monitoring of high-mountain terrain deformation and glaciers, respectively; Wessels *et al.* (2002) used ASTER images for analyzing supraglacial lakes at Mt. Everest. Cheng and Bean (2002) published first results about the generation of ASTER DEMs for Afghanistan. Eckert and Kellenberger (2002) compared two ASTER DEMs from mountainous regions in Switzerland with DEMs from InSAR data and the Swiss DEM25. For steep, forested terrain the calculated mean difference between the DEMs was only 15-23 m.

This paper compares the quality of two DEMs of the Cerro Sillajhuay in the Andes of Chile/Bolivia. One DEM was derived from contour maps (here: Contour DEM) and the other was derived from ASTER (here: ASTER DEM). Similar work has been done by Al-Rousan *et al.* (1997) and Al-Rousan and Petrie (1998), who compared a DEM derived from a SPOT stereo-pair with a DEM derived from contour maps (1:50,000 and 1:250,000), and found a very good agreement between both DEMs.

Fieldwork at the Cerro Sillajhuay was conducted only on the Chilean side during March and April 1998 and focused on geomorphological mapping after Kneisel *et al.* (1998) and Schröder and Makki (1998) with special respect to geomorphological processes as well as glacial and periglacial forms above 4300 m asl. (Bolch and Schröder, 2001). Aerial photographs with a resolution of approximately 2.5 m from 1961 were used for orientation and to monitor the geomorphological mapping. As fieldwork was not possible on the Bolivian side, a detailed, realistic geomorphological mapping of the entire study area is only possible with the help of DEM data.

Study Area

Cerro Sillajhuay (5982 m asl., 19°45' S / 68°42' W) is located in the Andes of Chile/Bolivia, and represents the highest peak of the Andes between 19 and 21 degrees south (Fig. 1). The stratovolcano is in a horst running crosswise to the main north-south orientation of the main Andes ridge as

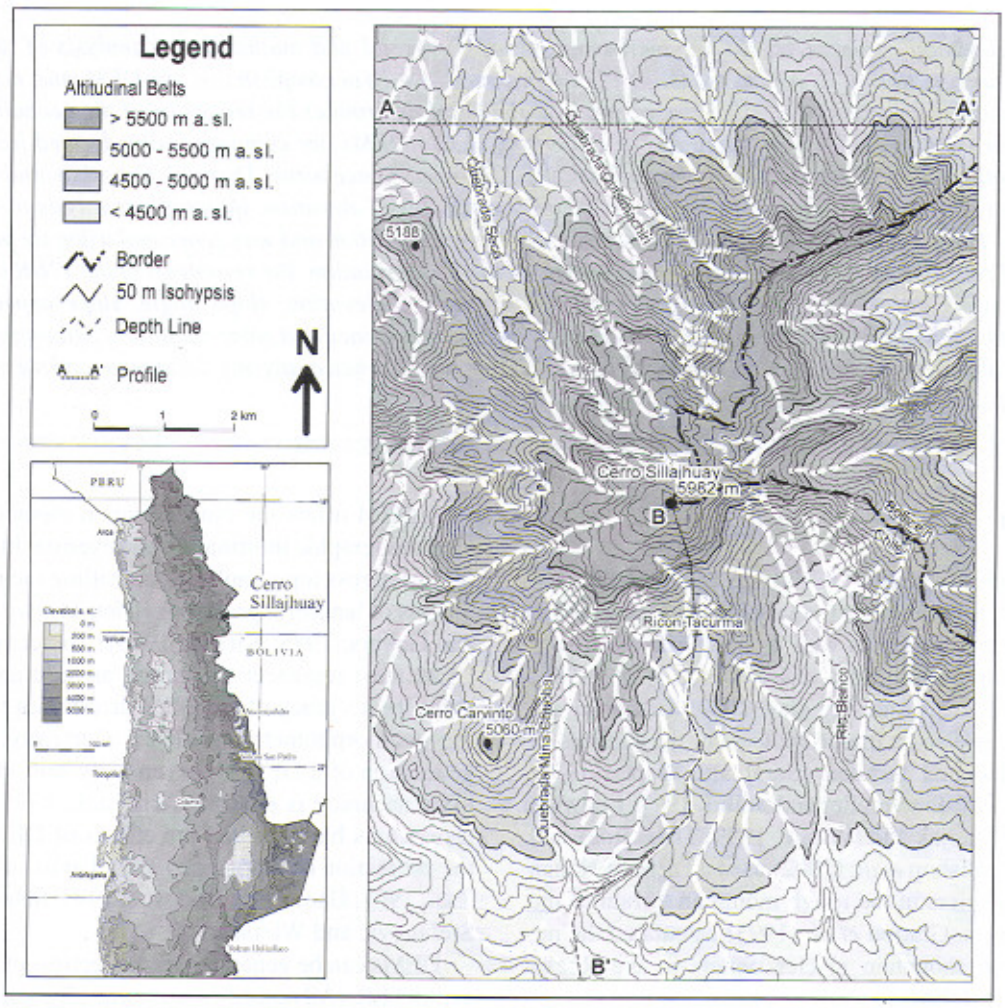

Figure 1 Location map of the study area in the Andes of Chile/Bolivia. For profiles A and B see Fig. 10.

a result of tectonic stress during uplift of the western Cordillera. It rises ~ 2000 m above the surrounding plain (Fig. 2), and is surrounded by several other volcanos. The median altitude of the massif is ca. 5030 m asl., and most of the terrain lies between 4750 and 5250 m asl. The ca. 3700-m high Salar de Coipasa and Salar de Uyuni on the Bolivian side represent the local erosion level. From here, the pediments smoothly slope up to the Cerro Sillajhuay massif, and only isolated hills break through the generally flat terrain. The massif itself is deeply incised by steeply sloping valleys. For example, the 2-km long Rio Blanco Valley ascends ca. 1100 m from mouth to peak. The ridge of the entire massif is more or less complete, and from here the relief plunges down to the valleys. In the southeast of the volcano lies Cancosa Basin at 3900 m asl., which was formerly covered by a lake (Schröder *et al.* 1999).

The study area is part of the Atacama, which is the driest part of the Andes; precipitation occurs in summer. Bolch and Schröder (2001) assume a precipitation of ca. 200 mm in 4500 m asl., and 300-400 mm in 5000 m asl. Cerro Sillajhuay itself is characterized by a local mountain climate with high diurnal variations in temperature and frequent days with frost-thaw-cycles. Discharge is orientated to the interior in the east. Vegetation cover is extremely sparse; grasses and shrubs are dominating and only isolated trees (*polylepis*) occur.

DEM from Contour Maps

DEM Generation and 3D-Visualization

Converting contour maps is a common way to create DEMs. For the Cerro Sillajhuay, a DEM was developed by digitizing contour lines from rectified topographic maps 1:50,000 with 50 m-equidistance (1945-6845 Pampa Lirima, 1945-6830 Cancosa, 1930-6845 Lagunas Chuncara, 1930-6830 Villa Blanca), which represent the best available maps for the study area. Additionally, depth lines and some ridges were digitized. Digitizing was carried out using a digitizing tablet and the software ArcView GIS 3.1 from ESRI. The DEM was developed in the Universal Transverse Mercator (UTM) projection, zone 19S, WGS 84. It covers an area of 10 x 17 km with the peak of Cerro Sillajhuay in its center.

Three calculation methods were tested for data interpolation: triangulated-irregular-networks interpolation (TIN), inverse-distance-weighted interpolation (IDW), and spline interpolation. Both IDW and spline method produced very good results for areas of high relief, but produced artifacts such as unrealistic low slopes in generally flat terrain. It seems that both methods had problems to handle larger distances between topographic contours. Best results were achieved by using the TIN method.

The first raw DEM contained many artifacts, mainly flat areas caused by the triangles, which are used by the TIN method for interpolation. Schneider (1998) and Rickenbacher (1998) published first solutions for their elimination, but the development of real 3D-breaklines is still a problem.

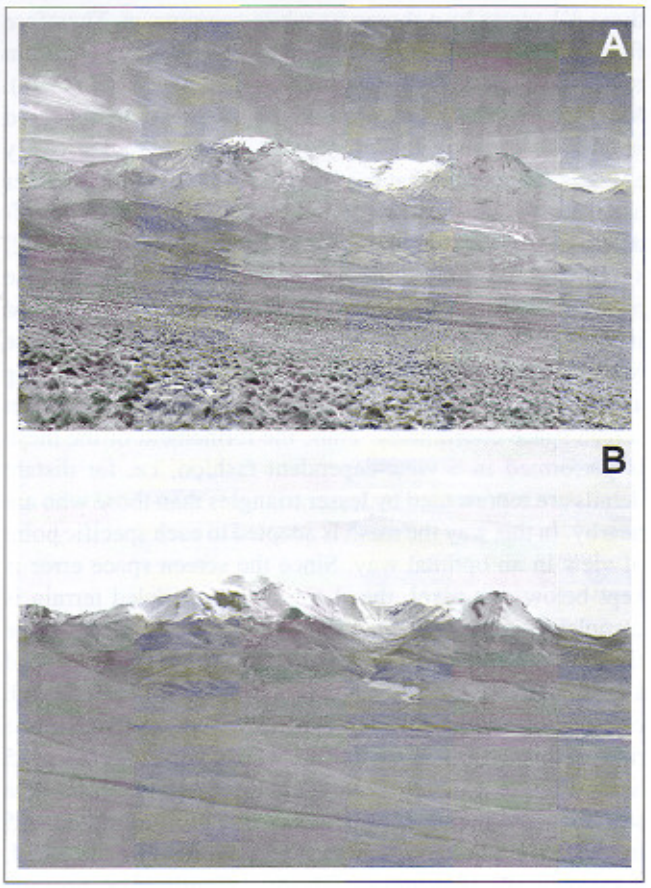

Figure 2 View across Cancosa Basin to Cerro Sillajhuay, a 5982-m high stratovolcano in the Andes of Chile and Bolivia: (A) photograph; (B) ASTER DEM. (Photo: G. Kröber, March 1998).

Therefore, in a second step some contour lines were manually added using information on elevation from stereoscopic analysis of the aerial photographs from 1961 with a resolution of 2.5 m. In the resulting DEM, nearly all artifacts could be eliminated. A disadvantage of the triangulation is the so-called diamond effect, i.e. each triangle has its own inclination and exposition, which impedes differentiation of such locations. Thus in a third step the TIN-DEM was converted into a grid-based DEM using the software ArcInfo 7.2 from ESRI. The grid-based DEM was smoothed two times using the 'quintic' filter, a nearest-neighbor algorithm of ArcInfo, and the 'grid generation tool', a nearest-neighbor filter of ArcView. The horizontal DEM grid resolution was set to 50 m, matching the underlying topographic map. It is a common problem in DEM generation that smoothing operations lead to generalization, i.e. a loss of some topographic details. For instance, Cerro Sillajhuay peak with a height of 5982 m in reality is only 5968 m high in the DEM. Also, some geomorphological forms such as edges, frost cliffs, and gorges disappear. All in all, the final DEM satisfactorily reflects reality and is of good use in visualization and mesoscalic geomorphologic analysis (Fig. 3a).

First, 3D-views of the DEM were created using the '3D-analyst' of the ArcView software (Fig. 3b). Unfortunately,

these 3D-views lose sharpness while zooming-in. Therefore further 3D-views were developed using an advanced terrain rendering approach as proposed by Röttger *et al.* (1998). Most terrain data sets are far too large to be rendered interactively, since the number of mesh triangles easily exceeds the amount that can be handled by modern graphics accelerators. As a work around the continuous-level-of-detail (C-LOD) technique (Akenine-Möller and Haines, 2002) simplifies the underlying triangular mesh such that the resulting reduced number of triangles can be processed interactively. This is accomplished by starting with a coarse representation of the mesh. Then the mesh is refined as long as the local error of the triangulation exceeds one pixel in screen space coordinates. Thus, the refinement of the mesh is performed in a view-dependent fashion, i.e. far distant details are represented by lesser triangles than those who are nearby. In this way the mesh is adapted to each specific point of view in an optimal way. Since the screen space error is kept below one pixel, the shape of the modeled terrain is completely preserved for visualization, while at the same time the number of generated triangles is reduced significantly. This property is essential for a thorough comparison of the DEMs. Typically, the achieved frame rates of this C-LOD algorithm are well beyond the critical 25 hertz, such that interactive explorations of the terrain data sets are made possible. By simulating a grid resolution of 5 m, the aerial photograph, which was overlaid on the DEM, preserves its sharpness. 'Fly-by' simulations provide additional information about the topography, morphometry and landforms of Cerro Sillajhuay.

Results

Generating DEMs from contour maps is easy, and the results provide reasonable information for geomorphological or hydrological interpretation. Unfortunately, it is often very time-consuming. Depending on the available topographic maps, DEMs of higher resolution and detail can be produced, which allows an analysis of the macro- and mesorelief, e.g. rock glaciers (Fig. 3c). For analyzing the microrelief, interpretation of aerial photographs produces better results.

ASTER DEM

Instrument and Data Set

ASTER is a high-spatial resolution, multi-spectral imaging system flying aboard TERRA, a satellite launched in December 1999 as part of NASA's Earth Observing System (EOS). An ASTER scene covering 61.5-km x 63-km contains data from 14 spectral bands. ASTER is comprised of three separate instrument subsystems representing different ground resolutions: three bands in the visible and near infrared spectral range (VNIR, 0.5-1.0 µm) with 15 m spatial resolution, six bands in the shortwave infrared spectral range (SWIR, 1.0-2.5 µm) with 30 m resolution, and five bands in the thermal infrared spectral range (TIR, 8-12 µm) with 90 m resolution. In the VNIR one nadir-looking (3N, 0.76-0.86 µm) and one backward-looking (3B, 27.6° off-nadir, taken ~ 60 sec. later) telescope provide black-and-white stereo images, which generate an along-track stereo image pair with a base-to-height ratio of about 0.6. The potential accuracy for the DEM from ASTER could be on the order of ±7 to ±30 m $RMSE_{xyz}$ (Long and Welch, 1999). ASTER is capable of recording 771 digital stereo pairs per day, and cross-track pointing out to 136 km allows viewing of any spot on Earth at least once every sixteen days.

One ASTER-level 1A scene, which, as per ASTER L1A specifications contains visible/near-IR, mid-IR, thermal-IR, and the matching aft looking near-IR data, acquired on May 28, 2001, was downloaded directly from the USGS EROS Data Center (EDC) EOSDIS Core System (ECS). Fortunately, Cerro Sillajhuay is located in the center of this image, which is absolutely cloud-free.

DEM Generation and 3D-Visualization

ASTER scenes are distributed in HDF-EOS format, which can be imported by the software OrthoEngine as part of the Geomatica 8.2 package from PCI Geomatics. Using this software, DEMs can be generated automatically. For DEM extraction only the VNIR nadir and backward images (3N and 3B) are used. The geometric model is a rigorous one; it reflects the physical reality of the complete viewing geometry and corrects distortions that occur in the imaging process due to platform, sensor, earth, and cartographic projection conditions. After rigorous models (collinearity and coplanarity equations) are computed for the 3N and 3B images, a pair of quasi-epipolar images is generated from the images in order to retain elevation parallax in only one direction. An automated image-matching procedure is used to generate the DEM through a comparison of the respective gray values of these images.

The quality of ASTER DEMs depends on the availability of tie points (TPs) and ground control points (GCPs) (PCI Geomatica User's Guide Version 8.2 October 2001). In this study, 12 TPs and 11 GCPs were collected between the stereo-pair using geo-rectified maps and aerial photos for identification of characteristic landforms such as moraines, rock glaciers and ridges that were surveyed in the field. The total horizontal RMS was < 1.17 pixel or < 17.5 m. The DEM was generated using PCI Geomatica, the only software at the time designated compliant with NASA's ATBD for ASTER DEMs, at 30 m resolution choosing the 'highest possible level of detail' function, and the holes were filled by choosing the 'automated interpolation' function. The overall quality of the DEM was outstanding, with only few artifacts mostly representing lakes. The DEM was re-sampled to 15 m to exploit full ortho-image resolution (Fig. 4a). The three-band VNIR nadir-looking image (1, 2, 3N) was orthorectified using the extracted DEM. Several perspective scenes and 'fly-by' simulations were developed showing the Cerro Sillajhuay from different views and in different scales (Figs. 4b, c).

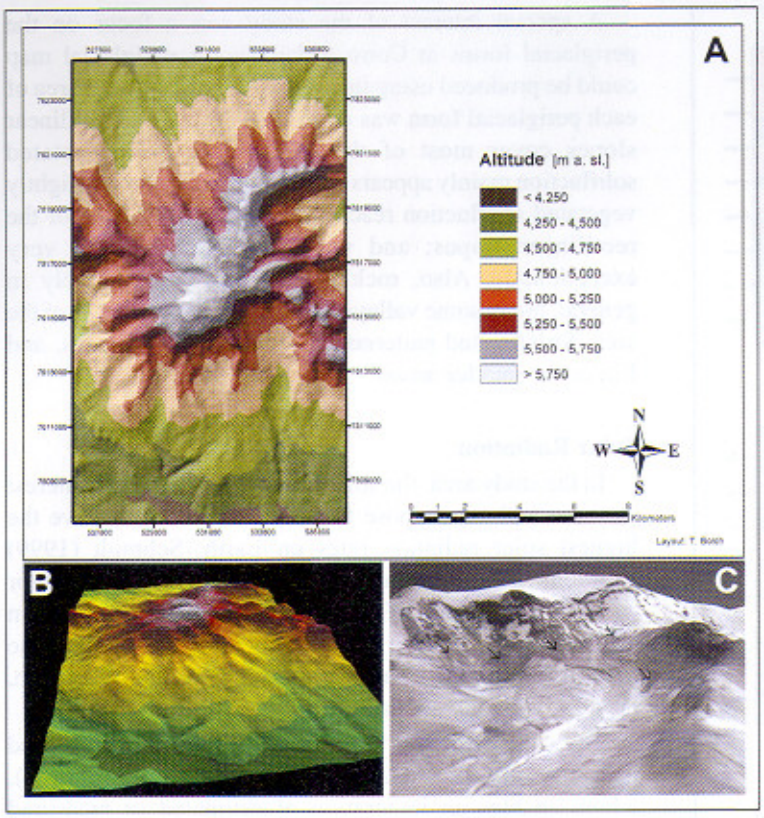

Figure 3 (A) Digital elevation model (DEM) of Cerro Sillajhuay derived from contour maps. (B) Virtual 3D-view. (C) Virtual 3D-view combined with aerial picture showing rock glaciers in the Tacurma Valley.

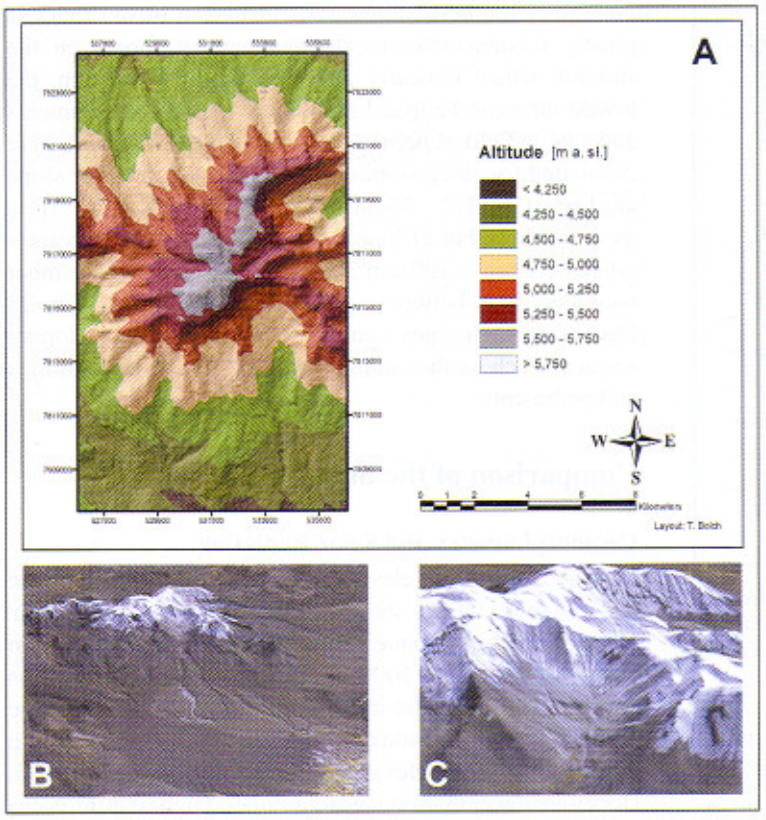

Figure 4 (A) Digital elevation model (DEM) of Cerro Sillajhuay derived from ASTER data. (B) Virtual 3D-view. (C) Virtual 3D-view of Rio Blanco Valley.

Results

The elevations in the ASTER DEM are of good accuracy and allow analysis of the macro- and mesorelief. Above 5000 m asl., elevations are too low due to internal smoothing procedures of the Geomatica software (elevations derived from ASTER DEMs in general are known to be often little too low; personal communication, PCI). Although particular elevation values may be too low, the developed 3D-views demonstrate the high quality of the DEM and the potential for more detailed morphometric image interpretation.

Thematic Analysis of the DEMs

Geomorphometry

The quality of both DEMs from contour maps and ASTER data was compared focusing on topography, geomorphology, morphometry, and landforms. Five geomorphic parameters, which are useful to identify and describe geomorphologic forms and processes, were extracted using the software ArcInfo and ArcView: elevation, aspect, slope angle, vertical curvature, and tangential curvature. Flow lines and the catchment areas of rock glaciers were extracted using the 'hydrologic modeling' tool 1.1, an extension of the ArcView software.

The elevation is graphically presented in a hypsometric map with eight classes, which at Cerro Sillajhuay at the same time represent altitudinal belts (Figs. 3a; 4a), e.g. the green class is vegetation cover, the yellow class is a transition zone, and the gray class represents firn fields.

Topography can be generalized into eight aspect classes, and this may also help to identify geomorphologic features (Fig. 5a). For example, differences in aspect may be an indicator of valley asymmetry.

Another map demonstrates the slope angle in six classes (Fig. 5b). The class with the lowest slope has a relatively steep upper boundary (5°) in accordance with the general relief, which comprises nearly no flat areas. Other slope classes may be useful to identify specific geomorphic forms: for example, rectilinear slopes (German: 'Glatthänge') have a slope of 25-35° per definition and should be found in the corresponding two classes of the slope map.

Slope curvature is of special interest for morphological and hydrological problems. Both curvatures are shown in maps of five classes: The vertical curvature is the second derivation of elevation regarding slope (Fig. 5c); and the tangential curvature is the second derivation of elevation relating to aspect (Fig. 5d). Obviously,

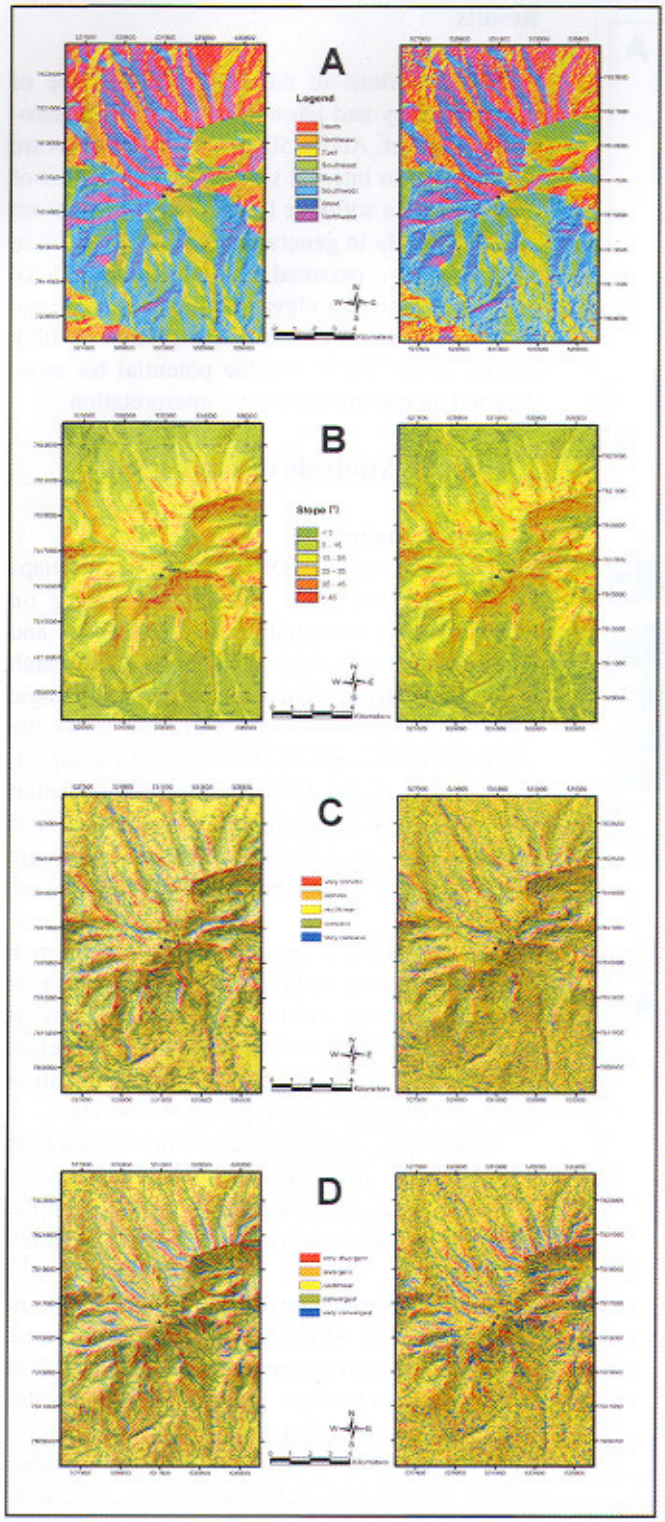

Figure 5 Morphometric parameters of Cerro Sillajhuay deriving from the Contour DEM (left), and from the ASTER DEM (right): (a) aspect, (b) slope angle, (c) vertical curvature, (d) tangential curvature. For elevation see Figs. 3a and 4a.

ridges have (very) convex and divergent profiles, and valleys have mostly (very) concave and convergent profiles. Mesoscale objects such as rock glaciers can be identified in several locations; the rock glacier front is characterized by a convex profile curvature and convex tangential curvature.

A special interest of the study was a focus on the periglacial forms at Cerro Sillajhuay. A periglacial map could be produced using the DEMs (Fig. 6), and the area of each periglacial form was calculated (Table 1). Rectilinear slopes cover most of the study area. Non-vegetated solifluction mainly appears on the rectilinear slopes; slightly vegetated solifluction reaches up to the lower limit of the rectilinear slopes; and vegetated solifuction is very exceptionally. Also, rock glaciers occur very rarely in general, but in some valleys they may cover up to 5 % of the area. Striated and patterned ground, breaking blocks, and firn cover smaller areas.

Solar Radiation

In the study area, the solar radiation is of special interest as some authors suppose that the Atacama may have the highest solar radiation rates on Earth. Schmidt (1999) mentions radiation values of 95 % of the solar constant for ca. 3700 m asl., and of 98 % at the Sairecabur, a volcano in northern Chile (5971 m asl., 22°43'S / 67°53'W). The reasons for these high values are low latitude, high elevation, dryness, and lack of nearly any clouds.

The solar radiation at Cerro Sillajhuay was computed using the software SAGA developed by Böhner *et al.* (1997), which enables an integration of estimated or measured atmospheric water vapor content and atmospheric pressure. In the map of solar radiation, areas of high radiation are easy to differentiate from areas of low radiation (Fig. 7). It is plausible that northern slopes receive higher radiation rates than southern slopes. The influence of the relief is plainly recognizable: the highest values appear on the summit, which is nearly always exposed to the sun; the lowest rates can be found at southern exposed escarpments and a large field of permanent snow. The lowest rates were calculated for steep slopes, and the highest rates for slope angles of ~ 15°. These values correlate with field measurements. For 21 June (winter) absolute radiation values range between ~ 200 and 3000 J/cm^2 and for 23 December (summer) it is between ~ 2000 and 3600 J/cm^2. On 23 December high rates can be found on slightly sloping surfaces such as the summit area, ridges, valley bottoms, and pediments.

Comparison of the both DEMs

Geomorphometry and Solar Radiation

When comparing elevation by using a difference image (Fig. 8), both DEMs show similar values up to ~ 4600 m asl. and nearly the same value for the minimum elevation (Table 2). Above ~ 5000 m asl., the calculated elevation from both DEMs differ increasingly with elevation, and the ASTER DEM elevations are slightly to low. In general, in the ASTER DEM elevations on overshadowed southern slopes are lower than on northern slopes. Highest differences do not occur at the peak but beneath the peak in southeast exposition. Beside this shadow effect the snowfields that

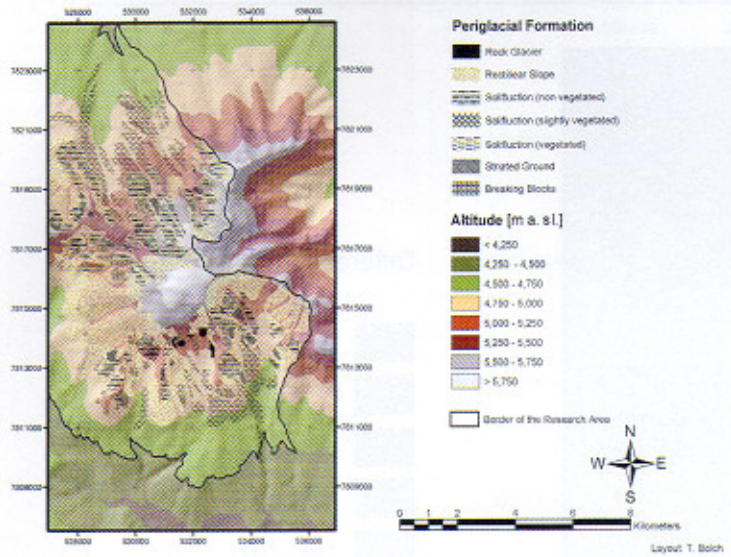

Figure 6 Periglacial map of Cerro Sillajhuay.

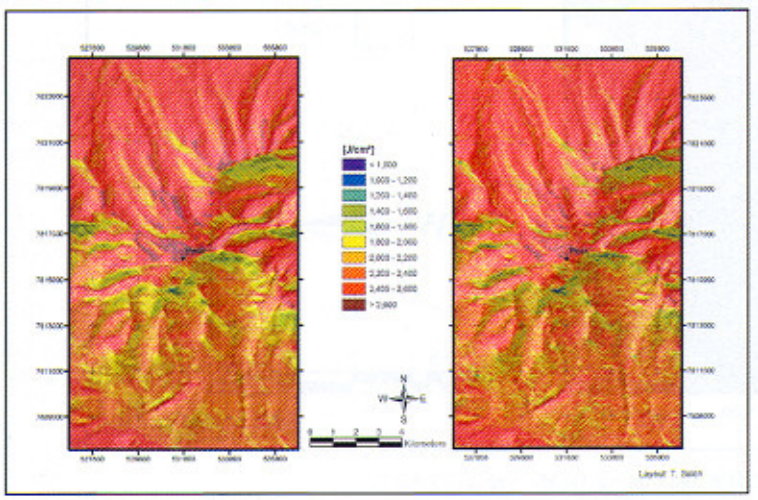

Figure 7 Map of the solar radiation at Cerro Sillajhuay derived from the Contour DEM (left) and the ASTER DEM (right).

set in above 5000 m influence the calculation. Other reasons might be the small number of available GCPs, and smoothing procedures of the Geomatica software.

Although the slope angles of both DEMs are generally similar (Fig. 5b), the ASTER DEM is more precise and reflects reality better. For example, the maximum slope angle of the steep cliff in the Tacurma Valley is 65°-70° from field measurements; in the ASTER DEM it is 61°, and in the Contour DEM it is only 52°. Compared to results from field mapping profile and tangential curvature are realistic in both DEMs, even though the ASTER DEM contains a few artifacts caused by perspective.

Topographic profiles were developed: one for the Tacurma Valley (Fig. 9a), and another one runs from W to E north of the summit (Fig. 9b). In general, the difference in calculated elevation from both DEMs increases with elevation. Whereas nearly no difference can be noticed in elevations below 4500 m asl., the difference increases above 4500 m asl. The ASTER DEM offers more detail of mesorelief.

Table 1 Areas for different periglacial forms.

Periglacial Form	Area in %
Rectilinear slopes	35.0
Rock glacier	0.3
Non-vegetated solifluction	11.0
Slightly vegetated solifluction	10.0
Vegetated solifluction	0.1
Striated and patterned grounds	1.5
Breaking blocks	2.5
Firn	2.0

Table 2 Main calculated indices for elevation from both Contour and ASTER DEMs. See also Fig. 11.

	ASTER DEM	Contour DEM
Mean Elevation	4842 m asl.	4931 m asl.
Maximum Elevation	5745 m asl.	5969 m asl.
Minimum Elevation	4182 m asl.	4189 m asl.
Standard Deviation	348 m	404 m
Difference ASTER DEM - Contour DEM		
Mean	- 89 m	
Maximum	+ 52 m	
Minimum	- 291 m	
Standard Deviation	59 m	

A more detailed analysis was undertaken for the rock glaciers in the Tacurma Valley. The slope angles of the catchment areas are similar for both DEMs, whereas the ASTER DEM offers more detail. By comparing the morphometry of the rock glaciers itself, the ASTER DEM shows more realistic results: the minimum slope angle of 5° matches the field measurements, and the maximum slope angle of 34° represents the general slope angle of active rock glaciers (35-40°). Knowledge about the geomorphometry is also important for a hydrologic modeling. Flow lines and surface run-off were calculated to delimit the catchment areas of the rock glaciers. In the measurement of area both DEMs show similar results, especially for the most active rock glaciers (Table 3: B1 and B2), even though the ASTER DEM seems to be more precise regarding the flow lines by comparing it with the virtual image (Fig. 10).

At Cerro Sillajhuay solar radiation is very high and extinction is very low according to its geographic position. The calculation of the mean daily solar radiation led to nearly the same rates for both DEMs (Table 4). For rock glaciers and especially their catchment areas, the lower minimum daily solar radiation rates for steep slopes calculated with the help of the ASTER DEM are more reliable.

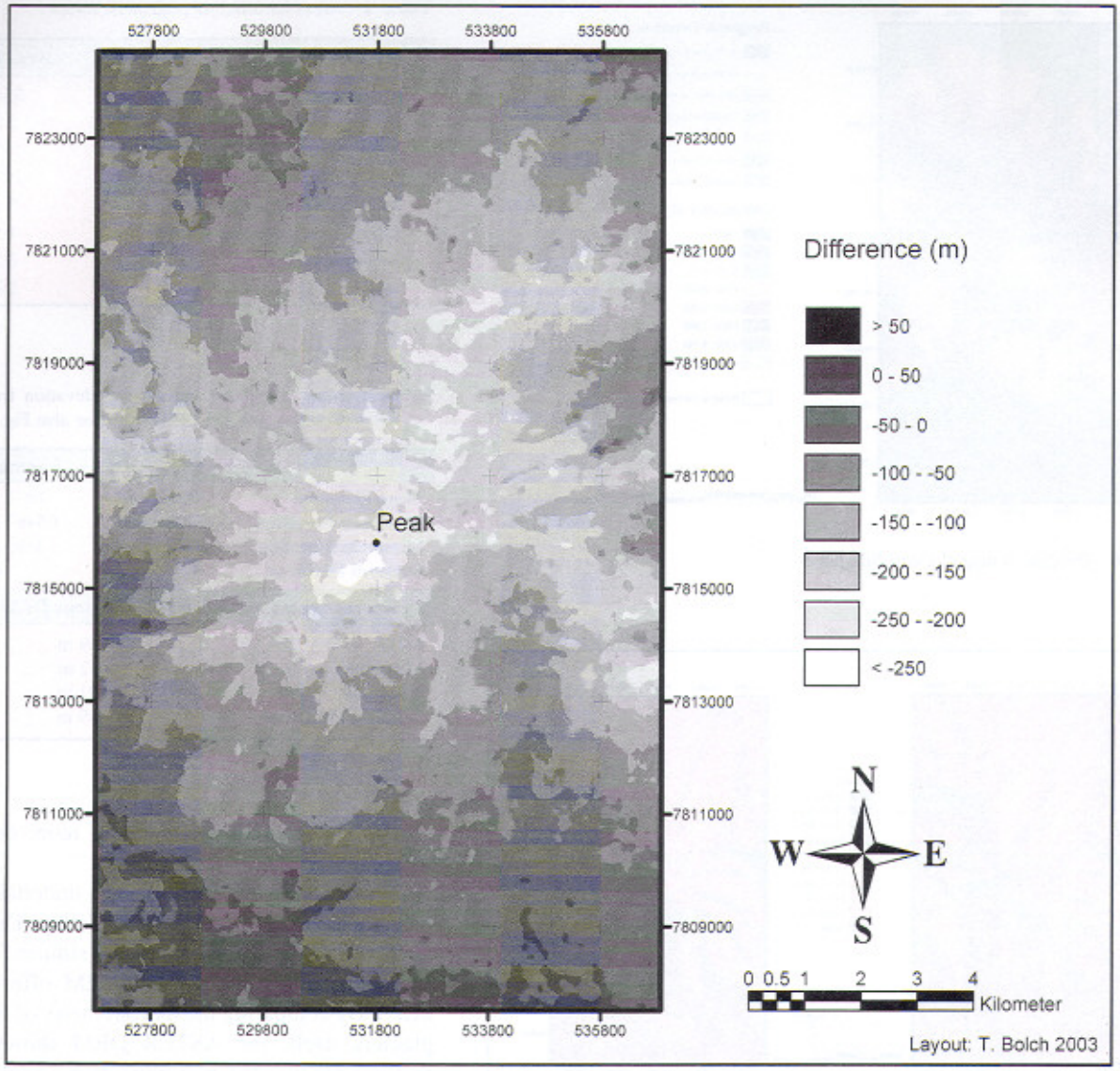

Figure 8 Difference image of elevation derived from ASTER and Contour DEMs. See also Table 2.

Table 3 Catchment areas of rock glaciers calculated from the Contour DEM and the ASTER DEM.

Rock Glacier	Contour DEM	ASTER DEM
B1	18.6 ha	17.2 ha
B2	79.5 ha	79.3 ha
B3	8.6 ha	6.7 ha
B4	69.8 ha	62.0 ha
B5	12.7 ha	14.9 ha

Discussion

Both DEM generation procedures have advantages as well as disadvantages. Regarding the Contour DEM, the digitalizing process of the contours is relatively time-consuming. Although software packages, which include an automated or semi-automated digitizing tool such as a line-following algorithm, are available, manual corrections are

Table 4 Solar radiation calculated from the Contour DEM and the ASTER DEM (in W/m2).

Daily Solar Radiation	Contour DEM (in W/m^2)	ASTER DEM (in W/m^2)	Rockglaciers Contour DEM (in W/m^2)	Rockglaciers ASTER DEM (in W/m^2) (in W/m^2)	Catchment Area Contour DEM (in W/m^2)	Catchment Area ASTER DEM
Mean	267	266	235	239	224	226
Minimum	134	88	193	189	134	88
Maximum	310	312	267	271	298	305

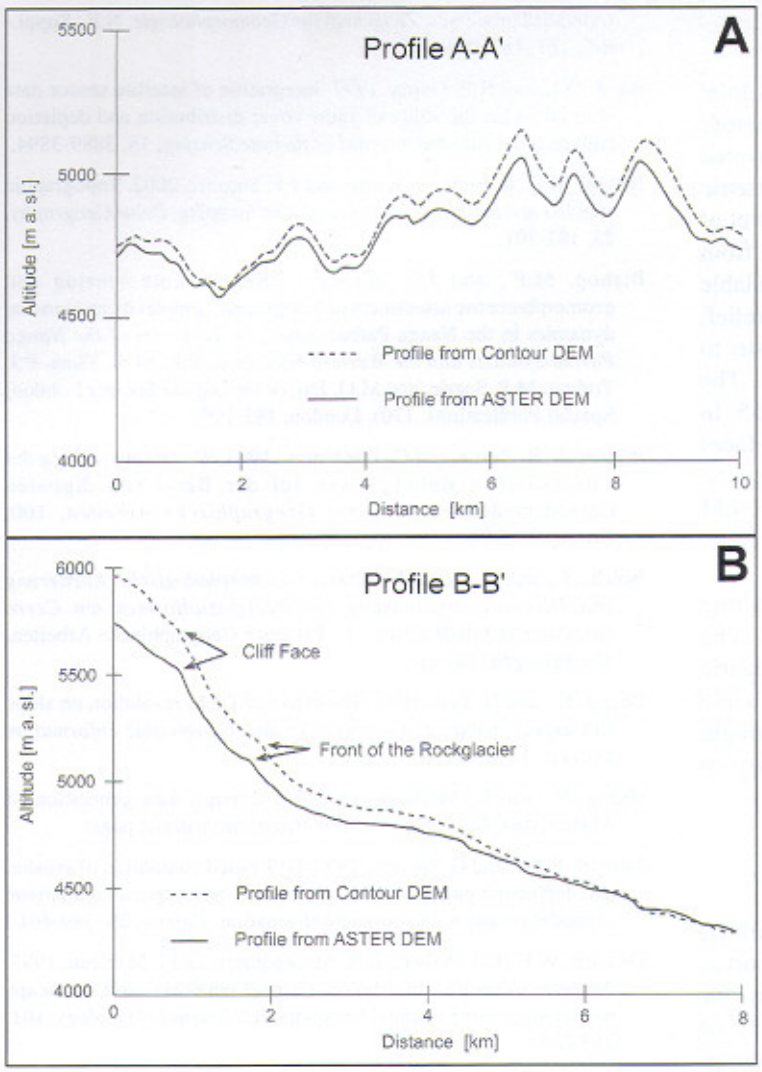

Figure 9 (A) Topographic W-E profile. (B) Topographic (longitudinal) profile of Tacurma Valley. For location of profiles see Fig. 1.

mostly necessary. The base maps themselves represent secondary data, which might contain errors. Furthermore, the interpolation methods, such as IDW, spline, or TIN, are more suitable for raster data than for vector data. On the other hand, it is easier to make changes in the interpolation algorithm such as using a different weight factor while developing a Contour DEM than while developing an ASTER DEM.

While developing an ASTER DEM by using a special commercial software package, the DEM developing algorithm cannot be changed easily. Often, the software offers only a few parameters for free selection by the operator. For identifying TPs, the operator needs experience in landforms and land covers, because the quality of the TPs/GCPs is essential for the DEM quality. But when familiar with the software, an operator can develop an ASTER DEM relatively quickly. ASTER DEMs are excellent for virtual-reality visualizations, because they represent quasi ortho-images.

Lang and Welch (1999) suggest that RMSExyz values for ASTER DEMs should be on the order of ±7 to ±30 m. DEMs produced in other mountainous areas have a preferential failure mode, i.e., facets with an aspect of 340 to 140 degrees or slopes over 35 degrees. This is likely due to two factors. First, relative to the ground being examined, the aft looking ASTER sensor is set at an azimuth of roughly 10 degrees, making slopes with an aspect of 10 degrees the least likely to be well imaged. Second, these slopes receive the least direct solar illumination, which, by reducing image contrast, increases the probability of image-to-image correlation failure.

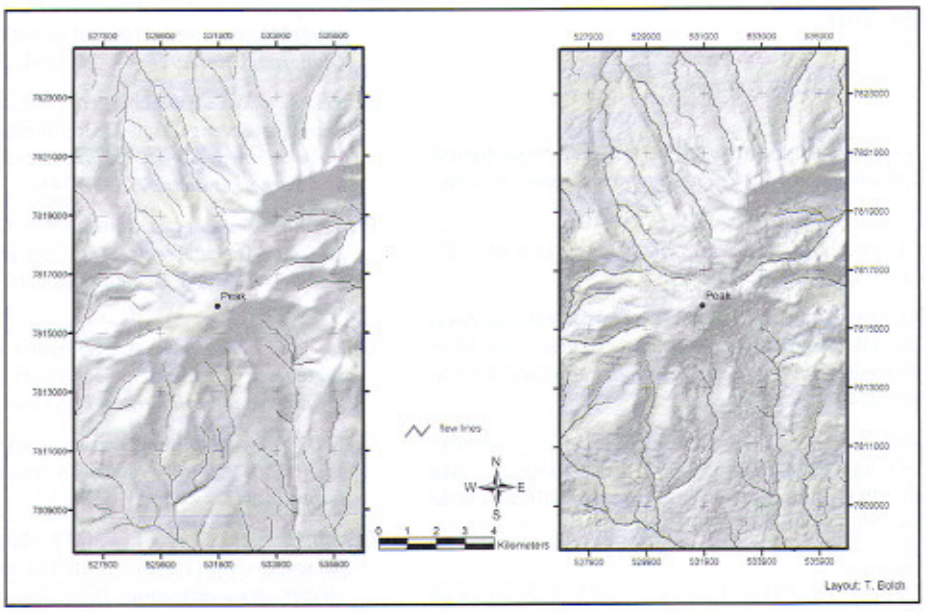

Figure 10 Map of flow lines at Cerro Sillajhuay using the Contour DEM (left) and ASTER DEM (right).

Conclusion

For Cerro Sillajhuay, a volcano in the Andes of Chile/Bolivia, DEMs were developed and analyzed by using contour maps and ASTER remote sensing data. The results presented here demonstrate that both DEMs are useful for morphometric analysis. The scale of a DEM sets the limits for the level of detail for geomorphologic analysis. Today, DEMs from ASTER remote sensing data and contour maps are reliable sources for an interpretation of the macro- and mesorelief, whereas ASTER DEMs offer more detail, are often easier to develop, and available for many parts of the Earth. The actual purchase price (2003) of an ASTER scene is $55. In general, the ASTER DEM is more accurate, e.g. cliff faces and steep slopes are easier to identify. Analyzing the microrelief requires a level of detail, which today's DEM resolutions deriving from satellite data do not offer. Here, aerial photographs still are the better choice.

ASTER data provides the opportunity for extracting elevation information from nadir and aft images. The simultaneous along-track stereo data eliminates radiometric variations caused by multi-date stereo data acquisition while improving image-matching performance. ASTER data might be useful for geomorphological mapping especially at medium scales (1:100,000 and 1:50,000).

Acknowledgements

The authors like to thank H. Schröder and G. Kröber, University of Erlangen-Nuremberg, Germany, for support in the field, J. Böhner, University of Göttingen, Germany, for solar radiation calculations, and S. Röttger, University of Stuttgart, Germany, for providing the interactive terrain renderer. The corresponding terrain-rendering library is distributed under the terms of the LGPL and can be downloaded from http://wwwvis.informatik.uni-stuttgart.de/~roettger. Part of this project was funded by the Max Kade Foundation, New York.

References

Abrams, M., and S.J. Hook, 1995. Simulated ASTER data for geological studies, *IEEE Transactions on Geoscience and Remote Sensing*, 33, 692-699.

Akenine-Möller, T, and E. Haines, 2002. *Real-time Rendering*, 2nd edition, A. K. Peters, Natick, 900 pp.

Al-Rousan, N., P. Cheng, G. Petrie, T. Toutin, and M.J. Valadan Zoej, 1997. Automated DEM extraction and orthoimage generation from SPOT level 1B imagery, *Photogrammetric Engineering and Remote Sensing*, 63, 965-974.

Al-Rousan, N., and G. Petrie, 1998. System calibration, geometric accuracy testing and validation of DEM and orthoimage data extracted from SPOT stereopairs using commercially available image processing systems, *International Archives for Photogrammetry and Remote Sensing*, 32, 8-15.

Band, L.E., R. Vertessy, and R.B. Lammers, 1995. The effect of different terrain representations and resolution on simulated watershed processes, *Zeitschrift fur Geomorphologie*, N.F., Suppl.-Bd., 101, 187-199.

Baral, D.J., and R.P. Gupta, 1997. Integration of satellite sensor data with DEM for the study of snow cover distribution and depletion pattern, *International Journal of Remote Sensing*, 18, 3889-3894.

Bishop, M.P., R. Bonk, U. Kamp, and J.F. Shroder, 2002. Topographic analysis and modeling for alpine glacier mapping, *Polar Geography*, 25, 181-201.

Bishop, M.P., and J.F. Shroder, 2000. Remote sensing and geomorphometric assessment of topographic complexity and erosion dynamics in the Nanga Parbat massif, in *Tectonics of the Nanga Parbat Syntaxis and the Western Himalaya*, Eds. M.A. Khan, P.J. Treloar, M.P. Searle, and M.Q. Jan, (= Geological Society London, Special Publications, 170), London, 181-199.

Böhner, J., R. Kothe, and C. Trachinow, 1997. Weiterentwicklung der automatischen Reliefanalyse auf der Basis von digitalen Gelandemodellen, *Göttinger Geographische Arbeiten*, 100, Gottingen, 3-21.

Bolch, T., and H. Schröder, 2001. *Geomorphologische Kartierung und Diversitätsbestimmung der Periglazialformen am Cerro Sillajhuay (Chile/Bolivien)*, (= Erlanger Geographische Arbeiten, 28), Erlangen, 141 pp.

Chang, K., and B. Tsai, 1991. The effect of DEM resolution on slope and aspect mapping, *Cartography and Geographic Information Systems*, 18, 69-77.

Cheng, P., and L. McBean, 2002. Fly-through data generation of Afghanistan, *Earth Observation Magazine*, without page.

Desmet, P.J.J., and G. Govers, 1995. GIS-based simulation of erosion and deposition patterns in an agricultural landscape: a comparison of model results with soil map information, *Catena*, 25, 389-401.

Dietrich, W.E., C.J. Wilson, D.R. Montgomery, and J. McKean, 1993. Analysis of erosion thresholds, channel networks, and landscape morphology using a digital terrain model, *Journal of Geology*, 101, 259-278.

Dikau, R., E.E. Brabb, R.K. Mark, and R.J. Pike, 1995. Morphometric landform analysis of New Mexico, *Zeitschrift für Geomorphologie*, N.F., Suppl.-Bd., 101, 109-126.

Duncan, C.C., A.J. Klein, J.G. Masek, and B.L. Isacks, 1998. Comparison of Late Pleistocene and modern glacier extents in central Nepal based on digital elevation data and satellite imagery, *Quaternary Research*, 49, 241-254.

Eckert, S., and T. Kellenberger, 2002. Qualitatsanalyse automatisch generierter digitaler Gelandemodelle aus ASTER Daten, *Publikationen der Deutschen Gesellschaft fur Photogrammetrie und Fernerkundung*, 11, 337-345.

Etzelmüller, B., and J.L. Sollid, 1997. Glacier geomorphometry - an approach for analysing long-term glacier surface changes using grid-based digital elevation models, *Annals of Glaciology*, 24, 135-141.

Giles, P.T., 1998. Geomorphological signatures: classification of aggregated slope unit objects from digital elevation and remote sensing data, *Earth Surface Processes and Landforms*, 23, 581-594.

Gao, J., 1997. Resolution and accuracy of terrain representation by grid DEMs at a micro scale, *International Journal of Geographic Information Science*, 11, 199-212.

Gratton, D.J., P.J. Howarth, and D.J. Marceau, 1990. Combining DEM parameters with Landsat MSS TM imagery in a GIS for mountain glacier characterization, *IEEE Transactions on Geoscience and Remote Sensing*, 28, 766-769.

Hodgson, M.E., 1995. What cell size does the computed slope/aspect angle represent?, *Photogrammetric Engeneering and Remote Sensing*, 65, 513-517.

Kääb, A., 2002. Monitoring high-mountain terrain deformation from repeated air- and spaceborne opitcal data: examples using digital aerial imagery and ASTER data, *Journal of Photogrammetry and Remote Sensing*, 57, 39-52.

Kääb, A., C. Huggel, F. Paul, R. Wessels, B. Raup, H. Kieffer, J. Kargel, 2002: Glacier monitoring from ASTER imagery: accuracy and applications, *EARSeL Proceedings, LIS-SIG Workshop, Berne, March 11-13, 2002*.

Kirkby, M.J., 1990. The landscape viewed through models, *Zeitschrift für Geomorphologie*, N.F., Suppl.-Bd., 79, 63-81.

Kneisel, C., F. Lehmkuhl, S. Winkler, E. Tressel, and H. Schroder, 1998. Legende für geomorphologische Kartierungen in Hochgebirgen (GMK Hochgebirge), *Trierer Geographische Studien*, 18, 1-24.

Krzystek, P., 1995. New investigations into the practical performance of automatic DEM generation, *Proceedings, ACSM/ASPRS Annual Convention, Charlotte, North Carolina, American Society for Photogrammetry and Remote Sensing*, 2, 488-500.

Lodwick, G.D., and S.H. Paine, 1985. A digital elevation model of the Barnes Ice-Cap derived from Landsat MSS data, *Photogrammetric Engineering and Remote Sensing*, 51, 1937-1944.

Long, H.R., and R. Welch, 1999. *Algorithm Theoretical Basis Document for ASTER Digital Elevation Models ver 3.0*, NASA Document ATBD-AST-08.

Millaresis, G.C., and D.P. Argialas, 2000. Extraction and delineation of alluvial fans from digital elevation models and Landsat Thematic Mapper images, *Photogrammetric Engineering and Remote Sensing*, 66, 1093-1101.

Raup, B.H., H.H. Kieffer, T.M. Hare, and J.S. Kargel, 2000. Generation of data acquisition requests for the ASTER satellite instrument for monitoring a globally distributed target: Glaciers, *IEEE Transactions on Geoscience and Remote Sensing*, 38, 1105-1112.

Rickenbacher, M., 1998. Die digitale Modellierung des Hochgebirges im DGM25 des Bundesamtes fuer Landestopographie, *Wiener Schriften zur Geographie und Kartographie*, 11, 49-55.

Röttger, S., W. Heidrich, P. Slusallek, and H.-P. Seidel, 1998. Real-time generation of continuous levels of detail for height fields, *Proceedings Sixth International Conference in Central Europe on Computer Graphics and Visualization, Plzen, Chech Republic*, 315-322.

Schmidt, D., 1999. *Das Extremklima der nordchilenischen Hochatacama unter besonderer Berucksichtigung der Hohengradienten*, (= Dresdner Geographische Beitrage, 4), Dresden, 122 pp.

Schneider, K., 1998. *Geomorphologisch plausible Rekonstruktion der digitalen Repräsentation von Geländeoberflächen aus Höhendaten*, Unpublished PhD-Thesis, University Zurich, Switzerland, 226 pp.

Schoorl, J.M., M.P.W. Sonneveld, and A. Veldkamp, 2000. Three-dimensional landscape process modelling: the effect of DEM resolution, *Earth Surface Processes and Landforms*, 25, 1025-1034.

Schröder, H., T. Bolch, and G. Krober, 1999. Limnische Sedimentationen des Holozäns im Becken von Cancosa (Provinz Iquique, Chile), *Mitteilungen der Frankischen Geographischen Gesellschaft*, 46, 217-229.

Schröder, H., and M. Makki, 1998. Das Periglazial des Llullaillaco (Chile/Argentinien), *Petermanns Geographische Mitteilungen*, 142, 67-84.

Sidjak, R.W., and R.D. Wheate, 1999. Glacier mapping of the Illecillewaet icefield, British Columbia, Canada, using Landsat TM and digital elevation data, *International Journal of Remote Sensing*, 20, 273-284.

Shi, J., 2001. Estimation of snow fraction using simulated ASTER data, *IAHS Publication*, 267, 120-122.

Stefanovic, P., and G. Wiersema, 1985. Insolation from digital elevation models for mountain habitat evaluation, *ITC Journal*, 3, 177-186.

Theakstone, W.H., and F.M. Jacobsen, 1997. Digital terrain modelling of the surface and bed topography of the glacier Austre Okstindbreen, Okstindan, Norway, *Geografiska Annaler*, 79 A, 201-214.

Tucker, G.E., F. Catani, A. Rinaldo, and R.L. Bras, 2001. Statistical analysis of drainage density from digital terrain data, *Geomorphology*, 36, 187-202.

Welch, R., T. Jordan, H. Lang, and H. Murakami, 1998. ASTER as a source for topographic data in the late 1990's, *IEEE Transactions on Geoscience and Remote Sensing*, 36, 1282-1289.

Wessels, R.L., J.S. Kargel, and H.H. Kieffer, 2002. ASTER measurement of supraglacial lakes in the Mount Everest region of the Himalaya, *Annals of Glaciology*, 34, 399-408.